Resonant Raman spectroscopy of disordered, amorphous, and diamondlike carbon

A. C. Ferrari* and J. Robertson

Department of Engineering, University of Cambridge, Cambridge CB2 1PZ, United Kingdom
(Received 23 October 2000; revised manuscript received 15 February 2001; published 26 July 2001)

The Raman spectra of a wide range of disordered and amorphous carbons have been measured under excitation from 785 to 229 nm. The dispersion of peak positions and intensities with excitation wavelength is used to understand the nature of resonant Raman scattering in carbon and how to derive the local bonding and disorder from the Raman spectra. The spectra show three basic features, the D and G around 1600 and 1350 cm^{-1} for visible excitation and an extra T peak, for UV excitation, at $\sim$1060 cm^{-1}. The G peak, due to the stretching motion of sp^2 pairs, is a good indicator of disorder. It shows dispersion only in amorphous networks, with a dispersion rate proportional to the degree of disorder. Its shift well above 1600 cm^{-1} under UV excitation indicates the presence of sp^2 chains. The dispersion of the D peak is strongest in ordered carbons. It shows little dispersion in amorphous carbon, so that in UV excitation it becomes like a density-of-states feature of vibrations of sp^2 ringlike structures. The intensity ratio $I(D)/I(G)$ falls with increasing UV excitation in all forms of carbon, with a faster decrease in more ordered carbons, so that it is generally small for UV excitation. The T peak, due to sp^3 vibrations, only appears in UV Raman, lying around 1060 cm^{-1} for H-free carbons and around 980 cm^{-1} in hydrogenated carbons. In hydrogenated carbons, the sp^3 C-H$_x$ stretching modes around 2920 cm^{-1} can be clearly detected for UV excitation. This assignment is confirmed by deuterium substitution.

I. INTRODUCTION

Carbon is unique in that simple changes in its local bonding can give rise to materials as diverse as diamond, graphite, fullerenes, carbon nanotubes, and disordered, nanostructured and amorphous carbons. These materials have a remarkable range of mechanical, electronic, and electrochemical properties and many possible applications.[1–3] It is thus very useful to develop fast, reliable, and nondestructive techniques to probe the key parameters that control their physical behavior.

We are interested in amorphous carbons. We define diamondlike carbon (DLC) as an amorphous carbon (a-C) or an hydrogenated amorphous carbon (a-C:H) with a significant fraction of sp^3 bonds. a-C:H often has a rather small C-C sp^3 content. DLC's with highest sp^3 content are called tetrahedral amorphous carbon (ta-C) and its hydrogenated analog ta-C:H. The key parameters of interest in such materials are (1) the sp^3 content; (2) the clustering of the sp^2 phase; (3) the orientation of the sp^2 phase; (4) any cross-sectional structure; and (5) the H content. The sp^3 content alone mainly controls the elastic constants, but films with the same sp^3 and H content but different sp^2 clustering, sp^2 orientation or cross-sectional nanostructure can have different optical, electronic, and mechanical properties.

Raman spectroscopy is a popular, nondestructive tool for structural characterization of carbons.[4–11] It is traditionally carried out at wavelengths in the blue-green spectral region (488–514.5 nm), but multiwavelength Raman (MW Raman) studies are becoming increasingly used. Indeed, Raman scattering from carbons is always a resonant process, in which configurations whose band gaps match the excitation energy are preferentially excited. Any mixture of sp^3, sp^2, and sp^1 carbon atoms always has a gap between 0 and 5.5 eV, and this energy range matches that of IR-vis-UV Raman systems.

This implies that understanding the resonant Raman process in carbon systems will give a powerful, fast means for their structural and electronic characterization. For example, MW Raman has recently been used to distinguish the metallic and semiconducting forms of single-wall carbon nanotubes.[12,13] It has also been used to investigate the origin of the peaks at $\sim$1150 cm^{-1} and $\sim$1450 cm^{-1} in nanocrystalline diamond.[14]

In amorphous and disordered carbons there are very few studies using multiple wavelengths. Graphite, disordered graphite, and glassy carbon were studied by MW Raman by Vidano *et al.*[16] and others,[17–22] Ramsteiner and co-workers,[23] Yoshikawa *et al.*,[24] Tamor *et al.*,[25] and Pocsik *et al.*[26] studied diamondlike a-C:H. Calleja *et al.*[15] made the first resonant Raman study of diamond, Wagner and co-workers[23,27] gave the MW Raman spectra of microcrystalline diamond and Bormett *et al.*[28] extended this to the UV.

The Raman spectra of all carbons show several common features in the 800–2000 cm^{-1} region, the so-called G and D peaks, which lie at around 1560 and 1360 cm^{-1} for visible excitation, and the T peak, seen for UV excitation at around 1060 cm^{-1}. The G and D peaks are due to sp^2 sites only. The G peak is due to the bond stretching of all pairs of sp^2 atoms in both rings and chains.[9] The D peak is due to the breathing modes of sp^2 atoms in rings. The T peak is due to the C-C sp^3 vibrations and appears only in UV excitation.

Although Raman spectroscopy of carbons has continued for 30 years, there have been significant advances in our understanding recently. Firstly, C-C sp^3 vibrations were directly detected by UV Raman spectroscopy.[29,30] This should allow the sp^3 content to be derived and it is a major motivation to study the UV Raman spectra of carbon films.[31–36]

The second major advance is the understanding of the origin of the D peak. It was empirically proposed that the D peak arises as a resonant Raman coupling to the phonon of wave vector q when it equals the wave vector k of the elec-

tronic transition excited by the incident photon.[37,38,21] We called this a $k=q$ "quasiselection rule," since it qualitatively explains the observed trends, but the physical mechanism behind the resonance was not fully understood.[9] Recently, Thomsen and Reich[39] showed that the D peak arises from a double resonant Raman process. The double resonance condition effectively corresponds to a $k=\frac{1}{2}q$ condition, rather than the previous $k\approx q$ condition, as can be derived straightforwardly from Ref. 39 given the relative size of the photon and phonon energies. Reference 39, however, proposes that any phonon mode satisfying the $k\approx\frac{1}{2}q$ condition can give rise to the D peak, irrespective of the symmetry. In this paper and Refs. 9, 37, and 38, it is important to note that the $k\approx\frac{1}{2}q$ condition does not affect our conclusions on the nature of the D peak and on which optical branch contributes to the peak,[9] in contrast to what is stated in Ref. 39. Reference 39 only generalizes the concept of L_a in case of graphite to being an interdefect distance.

A complete theory bridging between the double resonance in graphite and the dominant Raman intensities of the breathing modes of clusters of sixfold rings, both giving rise to the D peak in graphite and in amorphous carbons, does not yet exist. This possibly will have to consider in detail the transition between clusters and the crystalline counterpart. However, for disordered carbons, one can map the energy levels and vibration modes of carbon clusters onto those of graphite:[9] $1/L_a\Leftrightarrow k$ and $1/L_a\Leftrightarrow q$, where L_a is the cluster size or in plane correlation length. This is the basis to explain the origin and dispersion of the D peak in carbons and to derive the real space motions (breathing modes) of the phonons giving rise to this band.[9,40,41] We could thus propose a three-stage model to relate the visible Raman spectra of disordered and amorphous carbons to their local bonding.[9]

In contrast to graphite, there is little MW Raman data for amorphous carbon. This paper aims at filling this gap by providing Raman spectra of a wide range of amorphous carbon films, excited over a wider range of wavelengths than previous studies (5.41–1.58 eV, or 229–785 nm). We show that the peak dispersions in a-C, ta-C, ta-C:H, diamondlike a-C:H, and polymeric a-C:H can be considered as canonical cases in the ternary phase diagram of the disordered C:H system.[9,1] We propose to explain the trends in peak positions and intensities by extending our three-stage model[9] to spectra excited at many wavelengths. A main conclusion is that the spectra and their dispersion are characteristic of each type of carbon, while their single-wavelength Raman spectrum may be indistinguishable. We then show how a two-wavelength (visible-UV) study can provide most of the information on the fraction and order of sp^2 sites in carbons. UV Raman spectroscopy also directly probes the C-H bonding in carbons, which is not easily accessible by lower energy excitation.

II. EXPERIMENT

A. Samples

We have analyzed a variety of carbon samples. As we focus on general trends, we discuss only selected cases. A ta-C sample was grown by an S-bend filtered cathodic

vacuum arc (FCVA).[42] It has $\sim$88% sp^3, as determined by electron energy loss spectroscopy (EELS) and a uniform cross section, as shown by x-ray reflectivity.[43] A typical ta-C:H film was grown by an electron cyclotron wave resonance source, from C_2H_2 and had $\sim$30% hydrogen.[44] We then annealed the same sample in vacuum in 100 °C steps until complete graphitization, following the H content by hydrogen effusion measurements[45] and the sp^3 content by EELS.[46] This allowed us to follow the evolution of the Raman spectra in a system with known sp^3 and H content. Furthermore, unlike ta-C that only transforms at very high temperatures,[32] ta-C:H transforms more gradually with most changes occurring between 400 and 800 °C. An a-C sample with low sp^3 content and band gap was produced by magnetron sputtering.[47] Two a-C:H films were grown by plasma enhanced chemical vapor deposition from CH_4. One diamondlike a-C:H sample had 30–35 % H and $\sim$60% sp^3 content[46] and a Tauc optical gap of $\sim$1.5 eV. The other polymeric a-C:H sample had an estimated H content of 40–50 % and a gap of 3–3.5 eV.

All these films generally have a surface layer of lower density not exceeding 2 nm thickness,[43] a part from the sputtered a-C, but in this case the bulk properties are not markedly different from the surface ones.[43] Cross-sectional uniformity is crucial if we wish to relate UV Raman spectra to bulk properties, since UV excitation probes just the topmost $\sim$10–15 nm of the samples at 224 nm. UV Raman spectroscopy is thus the preferred technique to probe surface properties, e.g. when surface treatments are used.

B. Raman instrumentation

Unpolarized Raman spectra were acquired at $\lambda=229$, 244, 325, 351, 458, 514.5, 532, 633, and 785 nm (5.41–1.58 eV) using a variety of spectrometers. The UV Raman spectra at 229 and 244 nm were excited using an intracavity, frequency-doubled Ar ion laser and the 325 nm with a He-Cd laser. The spectra were collected using two Renishaw micro-Raman 1000 spectrometers on a 40X objective, with 229, 244, or 325 nm filters, and an UV-enhanced charge-coupled device (CCD) camera. The spectral resolution was about 4–6 cm^{-1} at 244 and 325 nm, but rose to 12–15 cm^{-1} for 229 nm excitation. All the UV spectra must be corrected by subtracting the system response signal, obtained by measuring a background spectrum with an Al mirror and normalizing to the atmospheric N_2 vibrations.

The power on the sample was kept well below 1 mW. Sample damage is an issue in Raman measurements, particularly for UV excitation. Raman spectra were thus collected by varying acquisition times, both with and without sample rotation. For the polymeric a-C:H samples a very small damage in the center of the laser spot was sometimes unavoidable. In order to be sure that the signal we measured is a genuine feature of a-C:H samples, we performed measurements with samples rotating at a very high speed ($>$3000 rpm) with a random XY movement superimposed. In this way acquisition times up to 60 s could be reached without any visible damage and no change of the signal shape. The spectra were the same as those derived with static extremely
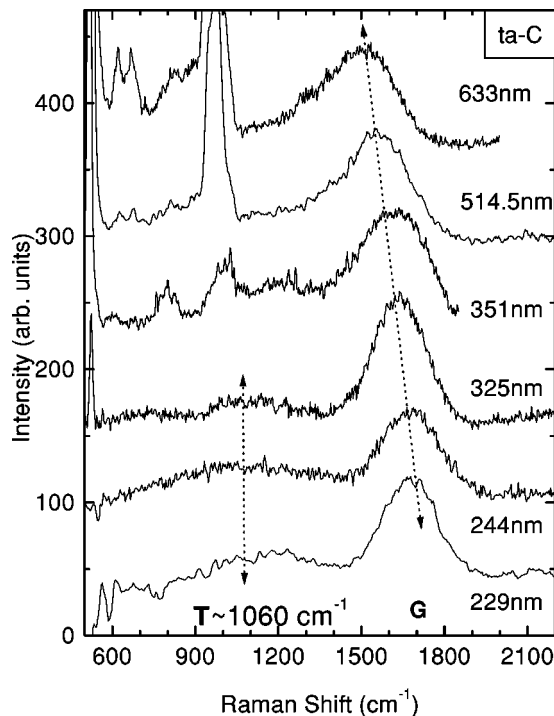
FIG. 1. MW Raman spectra of a ta-C sample with $\sim$88% sp^3. The G peak dispersion is indicated. The T peak at $\sim$1060 cm^{-1} is also shown; note that it does not disperse excitation energy, but just rapidly falls in intensity with decreasing excitation energy, as expected for an sp^3 VDOS. Note also the double structure which is evident at 325 nm excitation, with a lower frequency peak at $\sim$600 cm^{-1} (see text). For the lower excitation energies the contributions from the Si first- and second-order modes are also seen (Ref. 67).

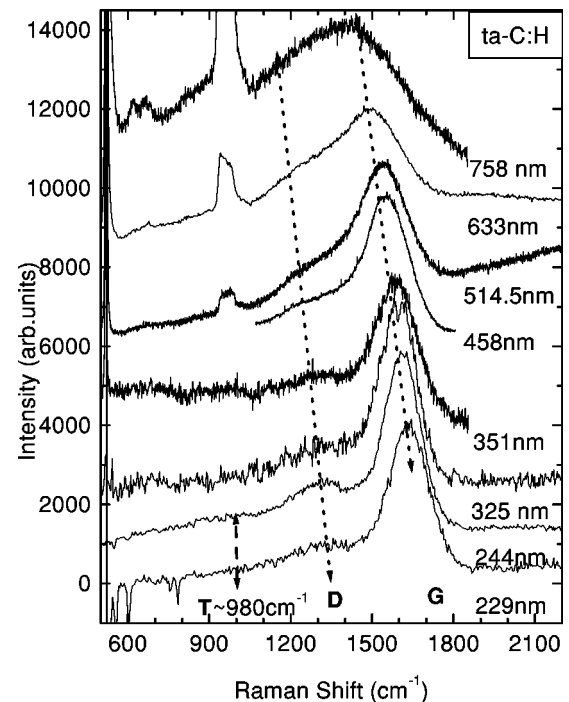

FIG. 2. MW Raman spectra of a ta-C:H sample with $\sim$70% sp^3 and $\sim$30% H. The G and D peaks' dispersions are indicated. The T peak at $\sim$980 cm^{-1} is also shown. Note that it does not disperse excitation energy, but just rapidly falls in intensity with decreasing excitation energy, as expected for an sp^3 VDOS. For the lower excitation energies the contributions from the Si first- and second-order modes are also seen (Ref. 67).

brief measurements (1–3 s long with less than 0.3 mW on the sample). We also measured less than 2-nm-thick a-C:H samples and yet obtained a similar spectral shape. Only longer acquisition times with no sample rotation caused clear damage, the main effect being an increase of intensity in the D peak region, followed by a general intensity drop corresponding to the sample being totally removed in the area of the laser spot. The reproducibility of the UV Raman spectra of a-C:H films when no visible damage was observed allows us to take them as representative of the material. Any possible local photoinduced transformation would happen in the micro-to nano-second range, but still allows us to distinguish the different starting materials.

Two other Renishaw systems with a 50$\times$ objective were used to acquire spectra at 514.5 nm (Ar ion laser), 633 nm (He-Ne laser), and 785 nm (diode laser). A Yobin-Yvon T64000 triple grating spectrometer with a 50$\times$ objective was used to acquire spectra at 514.5 nm (Ar ion laser) and 532 nm Nd-YAG laser. A Dilor *XY* with a 50$\times$ objective was used to acquire spectra at 458 and 351 nm from an Ar-ion laser but without a UV-enhanced CCD camera. This caused the 351 nm spectra to have lower quality than the 325 nm ones. Care was taken to avoid sample damage and typical resolution was 3–6 cm^{-1}.

We also tried to acquire spectra using an FT-Raman spectrometer at 1060 nm excitation. However, PL masks the Raman spectra for thin carbon films on Si.[48] This could be overcome by depositing samples on Al,[48] but we focus here on a well-characterized set of samples on Si. For this reason, most spectra at 785 nm for the less near-IR absorbing samples have a strong PL contribution and thus will not be considered further.

The least noisy spectra were acquired using Renishaw systems, thanks to the extended scanning and to the high CCD throughput. We will see how the trends in the Raman data are apparent over a few different excitations. Hence, as we are interested in peak dispersions over a broad energy range, we rely on the best spectra obtained with Renishaw systems.

III. RESULTS AND DISCUSSION

A. Spectra of canonical systems

Figures 1–7 show the Raman spectra of various samples. Figures 4 and 5 present the spectra of the ta-C:H sample annealed at 600 °C and at 1000 °C. ta-C:H has lost all its hydrogen and is completely graphitized by 1000 °C.[45,46] The hydrogen evolution and structural changes start at 600 °C and occur mostly from 600 to 800 °C.[45,46]

Figure 7 shows the spectra of the polymeric a-C:H. The increasing photoluminescence overshadows the Raman spectrum for excitation wavelengths over 351 nm. Thus, for polymeric a-C:H, UV excitation is needed for Raman studies.
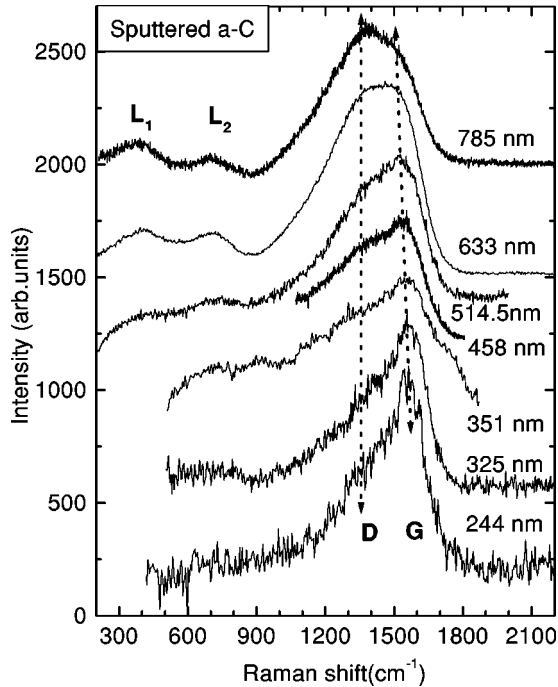
FIG. 3. MW Raman spectra of a sputtered a-C film with less than 20% sp^3. The G and D peaks' dispersions are indicated. Two extra peaks, L_1 and L_2, around 400 and 800 cm^{-1} are also indicated; these are typical of low sp^3 a-C (Refs. 68 and 66). We do not discuss them in this paper. For the other samples shown in the other figures, no other peak is evident in the low-frequency region, so this region is not plotted.

FIG. 4. MW Raman spectra of the ta-C:H film of Fig. 2 annealed post-deposition in vacuum at 600 °C. This temperature is the onset of major H effusion and sp^3 to sp^2 conversion (Refs. 45 and 46). The G and D peaks' dispersions are indicated. The T peak at $\sim$980 cm^{-1} is also shown. For the lower excitation energies the contributions from the Si first- and second-order modes are also seen (Ref. 67).

The drawback is the high absorption, which quickly leads to damage. However, we analyzed a series of samples with different band gaps from 2 to 3.5 eV and H contents from 18% to 37%.[49] A clear correlation between G position and the band gap and H content could be established,[50] showing that no significant damage is present, as discussed in Sec. II B. Note that very intense visible luminescence was observed for UV excitation in the most polymeric a-C:H; this luminescence was weak for diamondlike a-C:H and not observable for ta-C:H.

The spectra in general show three features, around 1560, 1360 (for visible excitation), and 1060 cm^{-1} (detected only in UV excitation), which are labeled as the G, D, and T peaks, respectively. The G and D peaks are due to sp^2 sites only. The G peak is due to the bond stretching of all pairs of sp^2 atoms in both rings and chains.[9] The D peak is due to the breathing modes of rings. The T peak is due to C-C sp^3 vibrations and appears only for UV excitation. The trends in the D, G, and T peaks are indicated in Figs. 1–7. Sections III B and III C focus on the trends in the G and D peaks. We will discuss the T peak in Sec. III E.

For visible excitation, the sp^2 sites have such a high cross section that they dominate the spectra, the sp^3 sites are invisible and the spectrum responds only to the configuration or order of the sp^2 sites. As the excitation energy rises, two effects occur, resonance causes the excitation of those sp^2 configurations with a wider gap, and then in the deep UV the modes of σ states of C-C bonds and C-H bonds are clearly seen.
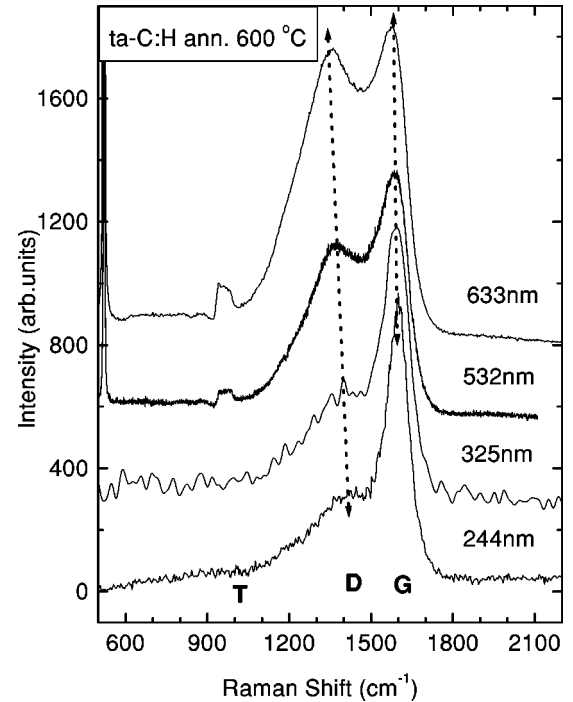
To obtain the positions and intensities of the G, D, and T peaks, we fitted the spectra using a combination of a Breit-Wigner-Fano (BWF) and a Lorentzian for the G and D peaks.[9] We used another Lorentzian for the T peak, when present. The peak position was chosen as the maximum of the BWF.[9] The BWF+Lorentzian combination for the D and G peaks is a convenient choice, since it provides good fits for all the carbons at all energies. We note that the skewness of the BWF strongly reduces going towards UV excitation, where it is not distinguishable from a Lorentzian. From Figs. 1–7 it is immediately clear that each system exhibits a different dispersion of G peak, D peak, $I(D)/I(G)$, and has a different $I(T)/I(G)$. We define $I(D)/I(G)$ and $I(T)/I(G)$ as peak heights ratios and not as peak areas ratios.

To rationalize these results we extended to multiwavelength excitation the three-stage model,[9] which was used to understand trends in the visible Raman parameters. This considers an amorphization trajectory consisting of three stages from graphite to Ta-C (or diamond): 1) graphite →nanocrystalline graphite (nc-G); 2) nanocrystalline graphite→$sp^2 a$-C; 3) a-C→ta-C($\rightarrow$100sp^3ta-C, defected diamond). Broadly, stage 1 corresponds to the reduction of the in-plane correlation length L_a within an ordered graphite layer. Stage 2 is the introduction of topological disorder into the graphite layer. Stage 3 is the conversion of sp^2 sites to sp^3 sites and the consequent change of sp^2 configuration from rings to chains.

We note that any features above $\sim$1360 cm^{-1} cannot be due to C-C sp^3 vibrations.[9] Thus, it is clear that the presence
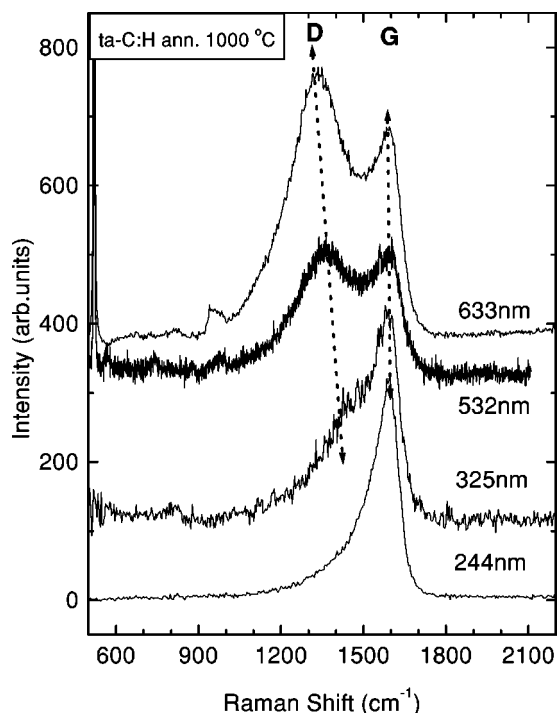
FIG. 5. MW Raman spectra of the ta-C:H film of Fig. 2 annealed in vacuum at 1000 °C. At this temperature complete H effusion and sp^3 to sp^2 conversion has happened (Refs. 45 and 46). The G and D peaks' dispersions are indicated. For the lower excitation energies the contributions from the Si first- and second-order modes are also seen (Ref. 67).

FIG. 6. MW Raman spectra of a diamondlike a-C:H sample with an sp^3 content of ~60%, Tauc optical gap ~1.5 eV and an estimated H content of 30–35 at. % (Ref. 46). The G and D peaks' dispersions are indicated. The T peak at ~980 cm^{-1} is also shown. For the lower excitation energies the contributions from the Si first- and second-order modes are also seen (Ref. 67).

of G peaks in Figs. 1–7 means that sp^2 vibrations still dominate even in the UV Raman excitation. In the following sections we will discuss the G, D, and T peaks, extending the three-stage model to multiwavelength excitation.

B. The G peak

Figure 8 shows the variation of G peak position with excitation wavelength and energy. Data on ta-C:H annealed at 400 and 500 °C are added for completeness; they resemble the G dispersion in a-C:H of different band gaps found by Tamor *et al.*[25]

The G peak does not disperse in graphite itself, nc-G or glassy carbon.[16–20,22,26] The G peak only disperses in more disordered carbon, where the dispersion is proportional to the degree of disorder. This is an important finding, by which the physical behavior of the G peak in disordered graphite is radically different from amorphous carbons, even though the G peak positions might accidentally be the same at some excitation energy. The G peak in graphite cannot disperse because it is the Raman-active phonon mode of the crystal. In nc-G, the G peak shifts slightly upwards at fixed excitation energy due to phonon confinement, but it cannot disperse with varying excitation energy, still being a density of states feature. The G peak dispersion occurs only in more disordered carbon, because now there is a range of configurations with different local band gaps and different phonon modes. The dispersion arises from a resonant selection of sp^2 configurations or clusters with wider π band gaps, and
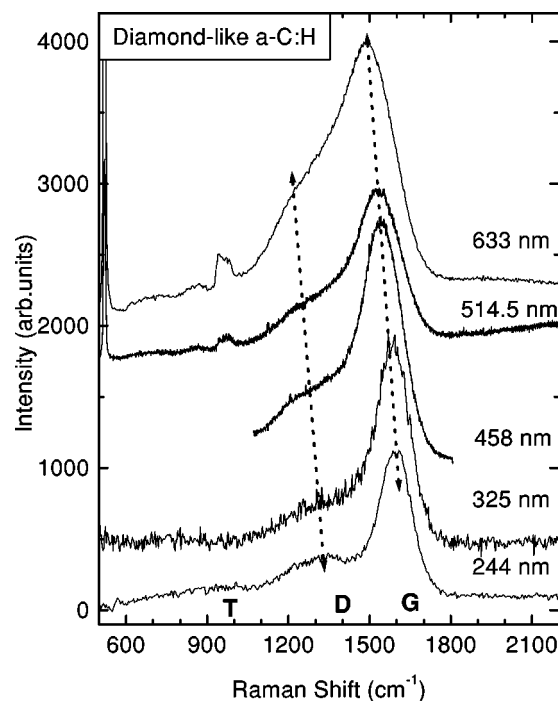
correspondingly higher vibration frequencies. A clear demonstration of this is seen in Fig. 9, which plots the G dispersion (in cm^{-1}/nm) against annealing temperature T_{ann} for ta-C:H. Here, the slope decreases with increasing T_{ann} because the disorder decreases.

The G peak dispersion separates the materials into two types. In materials with only sp^2 rings, the G peak dispersion saturates at a maximum of ~1600 cm^{-1}, the G position in nc-G. In contrast, in those materials also containing sp^2 chains, particularly ta-C and ta-C:H, the G peak rises past 1600 cm^{-1} and can reach 1690 cm^{-1} at 229 nm excitation in ta-C. This high G peak position can only be due to short, strained C=C bonded chains, if one notes that the C=C stretching vibration in ethylene is at ~1630 cm^{-1}. This is the first direct evidence of the presence of sp^2 chains in ta-C, so far only predicted in structural simulations.[51–53] Thus, UV Raman gives not only a more evenly weighted probe of sp^3 and sp^2 sites, but also an evenly weighted probe of rings and chains. It is not biased towards sp^2 configurations of lower band gap.

A similar dispersion of the C-C stretching modes occurs in transpolyacetylene.[54,55] In contrast, the C-C stretching modes have no dispersion in polyparaphenylene (σ-bonded chains of benzene rings).[56] This is because the π electrons are confined to each benzene ring, and do not delocalize along the chain.[56] Only the introduction of a heteroatom (or disorder) allows π delocalization and thus dispersion.[56]

Figure 8 shows that the G peak dispersion is roughly linear with the excitation wavelength, but not with excitation
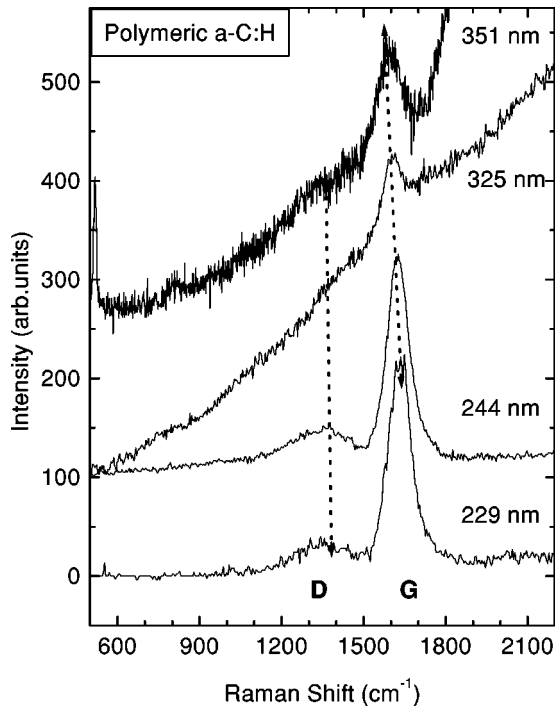
FIG. 7. MW Raman spectra of a polymeric a-C:H with an estimated H content of 40–50 at. % and a gap of 3–3.5 eV. Note the increasing PL background for decreasing excitation energy. Spectra collected at wavelengths longer than 351 nm just show the low energy PL tail (Ref. 9) and are thus not plotted. The G and D peaks' dispersions are indicated.
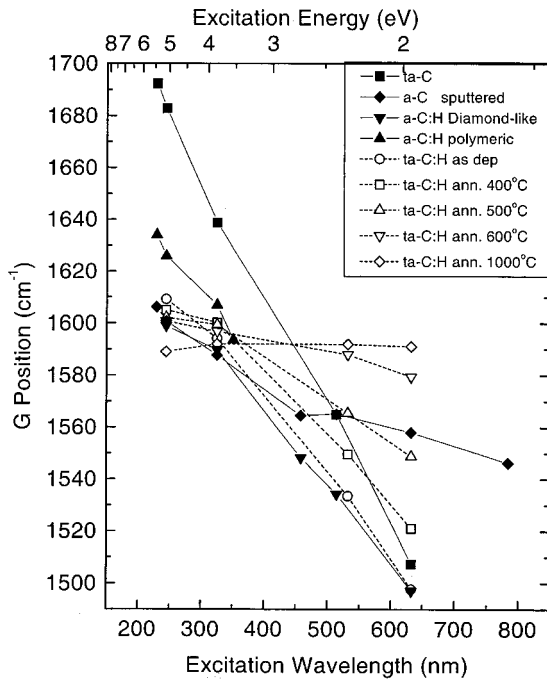

FIG. 9. G peak dispersion for ta-C:H samples annealed at increasing temperatures. The y axis is the slope (in cm^{-1}/nm) of the linear fit to the G position vs excitation wavelength data for ta-C:H of Fig. 8(a) and for the remaining annealing temperatures, not shown in Fig. 8(a).

energy. This is because the G mode upper limit is set by configurations with the widest band gap, which cannot be exceeded for a given structure, no matter how much we increase the energy. As the G dispersion is proportional to the degree of disorder, the G position becomes less sensitive to the gap with increasing excitation energies, since the gap is due to the more delocalized sp^2 structures.[1,9]

Figure 10 shows the full width half maximum (FWHM) of the G peak. The FWHM decreases with increasing excitation energy. This can be understood by noting that the gap of a-C is 0.5–1 eV and can reach 3.6 eV for ta-C. This means that a narrower distribution of higher gap sp^2 clusters

FIG. 8. Dispersion of G peak vs excitation wavelength (bottom x axis) and vs excitation energy (top x axis) for a series of template samples. The series of ta-C:H, as-deposited and annealed at various temperatures is marked by dotted lines.
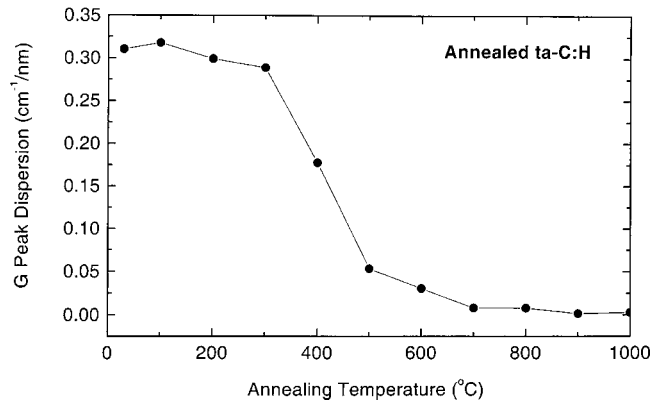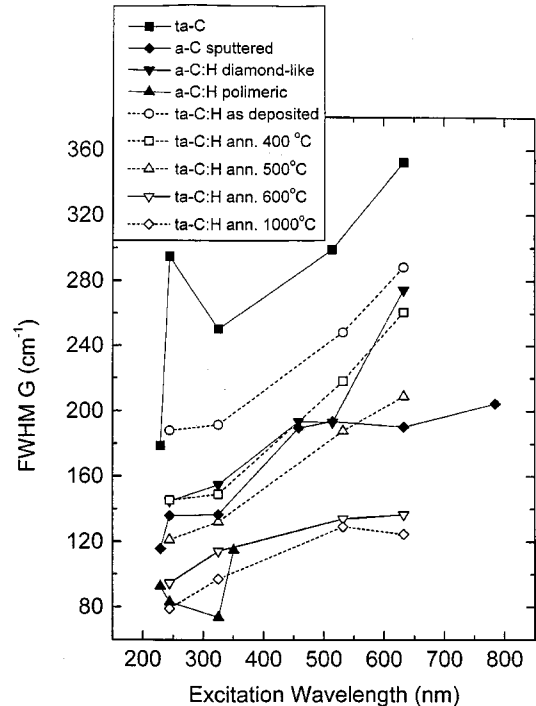

FIG. 10. Dispersion of the FWHM of the G peak for a series of template samples. The series of ta-C:H, as deposited and annealed at various temperatures, is marked by dotted lines.
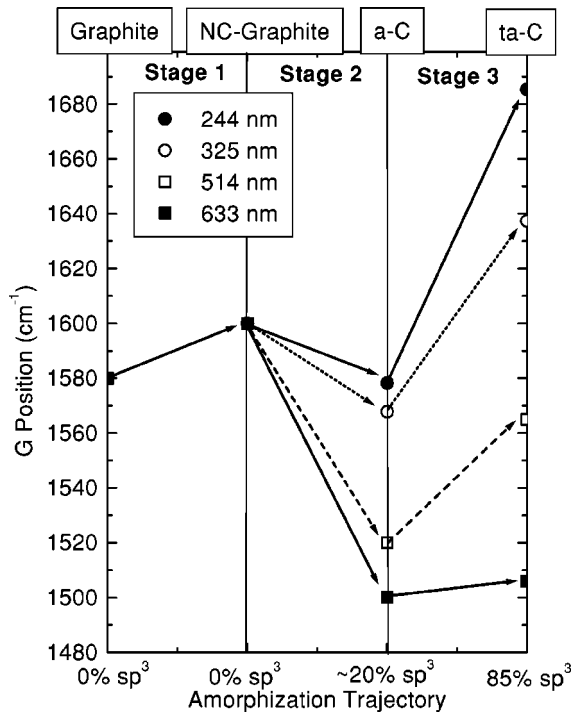
FIG. 11. Amorphization trajectory, showing the schematic variation of G position for four typical wavelengths.

is probed for increasing excitation energy, which results in a smaller width. Note also that at a fixed wavelength, ta-C has the largest G width, as it has the largest disorder or largest range of clusters. On the other hand polymeric a-C:H has a very narrow G peak, consistent with the low disorder in this material deposited at low ion energies.[1,57]

This range of behaviors of the G peak can be understood within the three-stage model,[9] as shown in Fig. 11 for four typical wavelengths.

In Ref. 9 we showed that following the reverse, *ordering* trajectory, from ta-C to graphite there can be hysteresis,[9] i.e., sp^2 clustering or π electron delocalization without a corresponding $sp^2 \rightarrow sp^3$ conversion. For visible excitation, sp^2 clustering and ordering will always *raise* the G peak in stages 2 and 3. In contrast, in UV excitation, increasing clustering *lowers* the G position, as noted above. This is shown schematically in Fig. 12. Comparing visible to UV excitation, there is an *inversion* of the trends. This is another remarkable result, since it allows for a distinction of samples that, although having different structures, may accidentally show very similar Raman spectra at a certain wavelength.

The detection of a trend inversion can be used to derive the amount of clustering of the sp^2 phase. If two samples have a similar G position in visible Raman spectra but very different ones in UV Raman spectra, the sample with the lower G position in the UV has more sp^2 clustering. A striking example of this is nitrogen introduction in S-bend FCVA ta-C films, for low N contents. There, to an almost zero change in the G position for 514 nm Raman spectra with increasing N content, corresponds a clear linear decrease of G peak in the UV Raman spectra, Fig. 13; this will be discussed with more detail elsewhere.
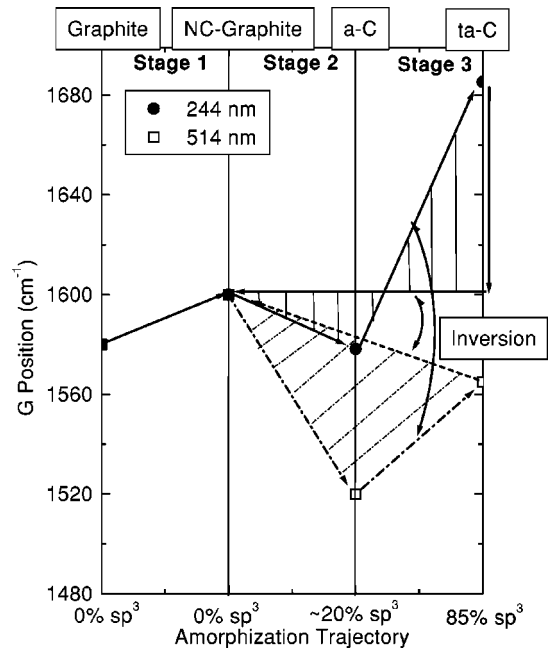

FIG. 12. Amorphization trajectory, showing the possibility of hysteresis in stages 2 and 3 for two typical wavelengths (514.5 and 244 nm). The regions span by hysteresis at 514.5 and 244 nm are evidenced by lines. Note the different shape of the hysteresis region for UV excitation: an *inversion* of the trends happens, with the highest shift Vis$\rightarrow$UV for samples having the least-ordered sp^2 phase (see text)

C. The D peak and $I(D)/I(G)$

The D peak arises from the breathing motion of sp^2 rings. $I(D)/I(G)$ is highest for IR excitation, and it decreases strongly at higher excitation energy. Although there is no D
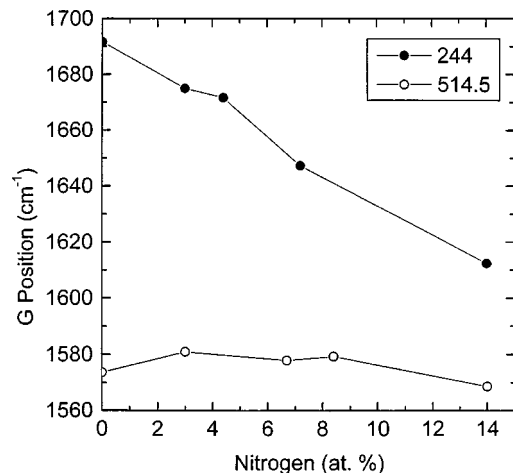

FIG. 13. G peak position (measured at 244 and 514.5 nm) vs nitrogen content (at. %) for ta-C:N samples deposited with a S-bend FCVA (Ref. 42). The nitrogen content was estimated from XPS (Ref. 42). Note that to an almost zero change of the G peak position at 514.5 nm, corresponds an almost linear decrease with N at 244 nm. This is a clear example of inversion (see text). MW Raman spectroscopy of N containing samples will be discussed in detail elsewhere.
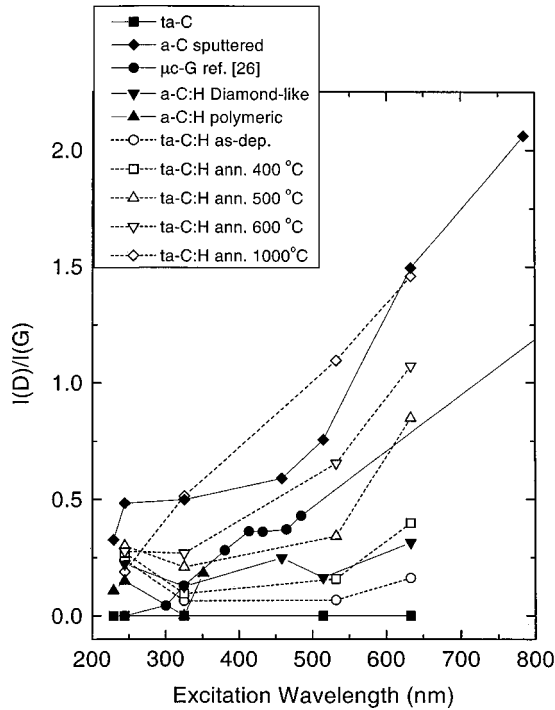
FIG. 14. Dispersion of $I(D)/I(G)$ vs excitation wavelength for a series of representative samples. The series of ta-C:H, as deposited and annealed at various temperatures is marked by dotted lines. Data on microcrystalline graphite from Pocksic *et al.* (Ref. 26) are added for completeness.
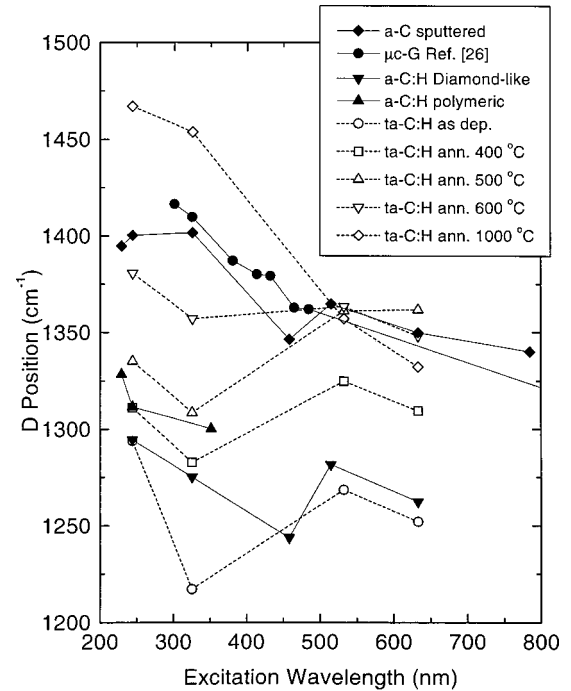

FIG. 15. Dispersion of D peak vs excitation wavelength for a series of representative samples. The series of ta-C:H, as deposited and annealed at various temperatures, is marked by dotted lines. Data on microcrystalline graphite from Pocksic *et al.* (Ref. 26) are added for completeness. Note that there is no D peak for ta-C at any wavelength.

peak in the UV Raman for nc-G graphite, Figs. 1–7 suggest that there is some residual intensity in the D region in UV Raman in the more disordered carbons, those with stage 2 disorder.

Figures 14 and 15 plot the $I(D)/I(G)$ intensity ratio and the D peak position as a function of excitation wavelength. Data of Pocsik *et al.*,[26] for microcrystalline graphite are added for completeness. In contrast to the G peak dispersion, the $I(D)/I(G)$ ratio and the D peak have maximum dispersion for microcrystalline and nanocrystalline graphite, and the dispersion decreases for increasing disorder, i.e., the dispersion is proportional to order.

The origin and dispersion of the D peak in disordered graphite arises from the $k=0.5q$ condition.[37–39,9] In particular, symmetric breathing modes have the highest modulation of the polarizability and thus the highest Raman cross section for $k=0.5q$.[9] Longer excitation wavelengths excite larger clusters with lower band gaps and lower frequency breathing modes. This is confirmed by calculations of Raman intensities of polycyclic aromatic hydrocarbons of increasing size, which exhibit two main bands corresponding to the G and D peaks in graphite.[40,41]

As disorder increases, the $I(D)/I(G)$ ratio disperses less. This means that the D peak disappears for UV excitation in disordered and nanocrystalline graphite, but not for amorphous carbons. This is clear, e.g., comparing ta-C:H annealed at 600 and 1000 °C in Figs. 4 and 5. Indeed for large disorder, as in sputtered a-C of Fig. 3, the D peak behaves like a nondispersive vibrational density-of-states feature for

the breathing modes of all ringlike sp^2 configurations. As far as we know, the presence of a residual D peak in UV Raman spectra of a-C's is a new finding, which can affect our deriving sp^3 content from the T peak, as discussed later. The presence of a D peak in UV excitation of a-C's is consistent with the UV Raman spectra of aromatic hydrocarbons. These show a clear D peak due to the ring breathing modes, and by varying the UV excitation, one can tune into a hydrocarbon with a given band gap.[58]

The $I(D)/I(G)$ ratio is widely used to estimate the sp^2 "grain" size from the Raman spectra via the Tuinstra-Koenig relation[5] for stage 1 disorder and its complement[9] for stage 2 disorder. Figure 14 shows that microcrystalline graphite of Ref. 26 always has a lower $I(D)/I(G)$ than the nc-G formed by annealing ta-C:H to 1000 °C. From the Tuinstra and Koening relation[5] for stage 1, this means that the microcrystalline graphite has larger grains. On the other hand, ta-C:H films annealed at lower T have a smaller $I(D)/I(G)$, because now, in stage 2, $I(D)/I(G)$ is less for smaller grains or more disorder.

Ideally, for an excitation energy E_{ex} we expect clusters of size $L \propto 1/E_{ex}$ to give the largest contribution. Thus, for the highest E_{ex}, a-C with the smallest aromatic clusters will have the highest $I(D)/I(G)$ with respect to nc-G. On the other hand the $I(D)/I(G)$ ratio is bigger for bigger clusters, as shown by *ab initio* calculations of Raman intensity,[41] thus explaining the overall decrease in $I(D)/I(G)$ intensity for increasing excitation energy. Furthermore, very disordered amorphous carbons have a specific size distribution of
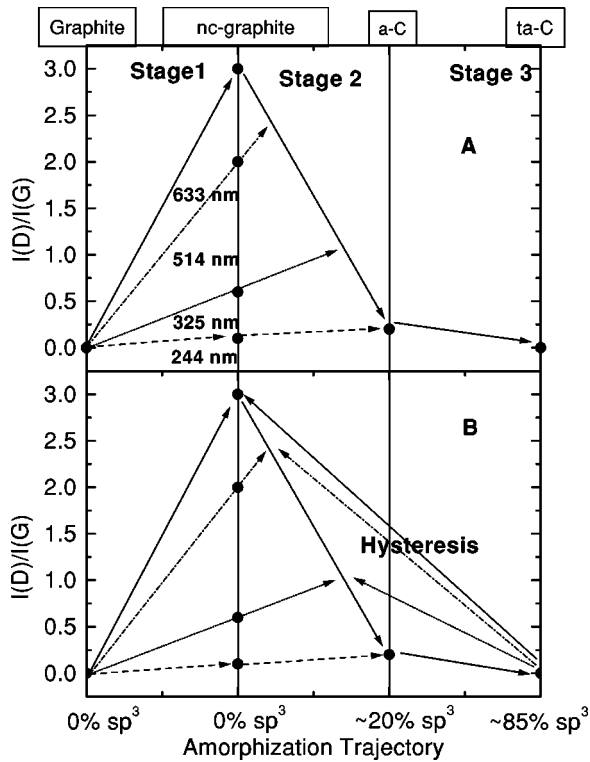
FIG. 16. (a) Amorphization trajectory, showing the schematic variation of $I(D)/I(G)$ for four typical wavelengths. Note that for increasing excitation energy, the maximum of $I(D)/I(G)$, corresponding to the transition between stage 1 and 2 shifts to higher disorder, i.e., lower L_a (see text). Note also that $I(D)/I(G) > 0$ for a-C even at UV excitation. (b) Amorphization trajectory for $I(D)/I(G)$, showing the possibility of hysteresis.

clusters, and cannot span all the breathing mode frequencies of clusters of rings of arbitrary size, unlike in defected graphite, where all the upper optical branch is spanned by the double resonance condition for varying excitation energies. We therefore expect an almost constant $I(D)/I(G)$ and D position for a-C. This is indeed seen experimentally, in Figs. 14 and 15. In ta-C, there is no D peak at any wavelength, due to a complete absence of rings.

These trends in $I(D)/I(G)$ can be summarized by extending the three-stage model to many wavelengths, as in Fig. 16(a). Note that the maximum of $I(D)/I(G)$ vs L_a shifts to smaller L_a for increasing E_{ex}, as seen in Fig. 16(a). Figure 16(b) shows the effect of hysteresis.

D. Hydrogen features

Figure 17(a) plots the first and second-order 229 nm Raman spectrum of a polymeric a-C:H film. There is a clear broad peak at ~ 2920 cm^{-1}. This corresponds to sp^3C-H$_x$ stretching modes, with a main contribution of sp^3C-H$_2$ and sp^3C-H groups.[57,59,60] To investigate C-H modes further, we deposited samples from CH$_4$ and CD$_4$.[61] Figures 17(b) and 17(c) compare the first and second-order region for a-C:H and a-C:D samples. It is seen that the band at ~ 2920 cm^{-1} shifts to ~ 2100–2200 cm^{-1}, confirming the assignment to C-H

stretching. Thus UV Raman scattering can give complementary information to FTIR for the H bonding.

If stretching vibrations are seen, we could expect to see the corresponding bending vibrations, as in FTIR spectra. The peak at ~ 1330 cm^{-1}, provisionally labeled as D, would then be a combination of a real D peak and C-H bending modes.

A closer look at Fig. 14 shows that for hydrogenated samples, while $I(D)/I(G)$ overall decreases with increasing excitation energy, there seems to be a minimum around 325 nm, and then a slight increase at higher E_{ex}. There could be two reasons for the increase. First, it could be due to the fitting procedure, given the extremely small $I(D)/I(G)$ for deep UV excitation and the appearance of the T peak. Second, as this occurs in H-containing films, it could be due to C-H bending modes, which lie in this region. Neutron scattering data of Honeybone et al.[62] and calculations of vibrational modes in model structures compatible with hydrogenated carbon materials[63,64] suggest that C-H bending modes lie near 1330 cm^{-1}. On the other hand, although slight changes in shape and intensity are observed for the ~ 1330 cm^{-1} peak in a-C:D, there is no significant downshift needed for pure C-H bending modes. This peak is thus mainly due to C-C vibrations and we will retain its assignment as a D peak.

Deuteration also causes a downshift of ~ 15 cm^{-1} of the G peak and ~ 30 cm^{-1} of the $2G$ peak. This shows that there is a small contribution of C-H bending to the C-C stretching vibrations in the G peak in hydrogenated samples, as expected for a material with hydrogenated sp^2 chains.[54] It could be argued that the ~ 1330 cm^{-1} peak arises from sample damage; however the carefulness of the measurements and the fact that we found a close correlation between Raman peaks and optical gaps for a series a polymeric a-C:H films[50] suggests that damage is negligible. Indeed, a clear dip around 1500 cm^{-1} is a typical fingerprint of polymeric a-C:H, as it does not occur in ta-C:H or diamondlike a-C:H. Another contribution in this region arises from the high-frequency tail of the T peak.

Figure 18 compares the 244-nm UV Raman spectra of ta-C, ta-C:H, and polymeric a-C:H, with the peak fits adopted in this paper.

The FTIR spectra of ta-C:H, diamondlike and polymeric a-C:H show a strong contribution at ~ 1450 cm^{-1} due to sp^2 CH aromatic and sp^3 CH$_3$ asymmetric or sp^3 CH$_2$ scissors modes.[57] This has no counterpart in the UV Raman spectra. However, we showed how the CH stretching modes are detectable in the UV Raman spectra of hydrogenated carbons. Further studies will be done to derive the CH contributions to the UV Raman spectrum and to fully analyse a full analysis of deuterated samples. This confirms our previous detection of SiH stretching modes in UV Raman spectra of ta-C:H:Si.[35]

To summarize, there are two possible contributions to the spectra around 1350 cm^{-1}, a true D peak due only to aromatic clusters of sixfold rings of sp^2 sites, and an almost nondispersive contribution in amorphous carbons from all sp^2 ringlike structure. The direct contribution of C-H bending modes appears to be negligible.
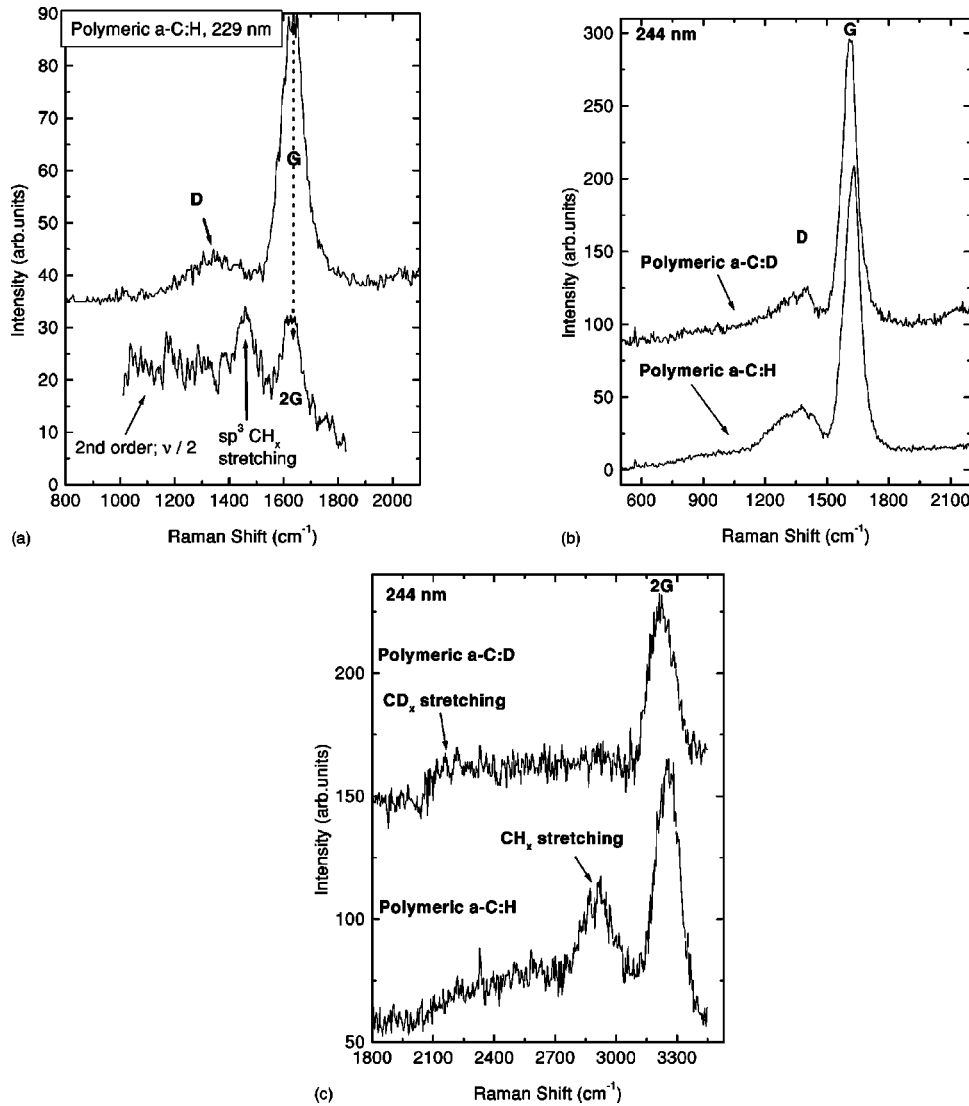
FIG. 17. (a) 229-nm Raman spectrum of the polymeric a-C:H. The bottom spectrum is the second-order region plotted vs $\frac{1}{2}$ of the Raman shift, in order to compare it with the first-order region. Note the $2G$ peak exactly corresponding to the G peak and the sp^3 CH$_x$ stretching at $\sim 2920/2$ cm^{-1}. (b) Comparison of the 244-nm Raman spectra of polymeric a-C:H and a-C:D samples. Note the downshift of ~ 15 cm^{-1} in the G peak of the a-C:D sample. Note as well that, although slight changes in shape and intensity are observed for the ~ 1330 cm^{-1} peak in a-C:D and a-C:H, the significant downshift in a-C:D, due to happen if this peak was due to pure C-H bending, is not observed, (c) Comparison of the second-order region of the 244 Raman spectra of polymeric a-C:H and a-C:D samples. Note the downshift of the ~ 2920 cm^{-1} band to ~ 2100–2200 cm^{-1}, as expected for a C-H stretching. Note as well the downshift of ~ 30 cm^{-1} of the $2G$ peak upon deuteration.

E. The T peak and sp^3 content

The first UV Raman studies of ta-C by Gilkes et al.[29] and Merkulov et al.[30] found a new peak at ~ 1060 cm^{-1} labeled T. This peak, seen only in UV excitation, is due to a resonant enhancement of the σ states, and it directly probes the sp^3 bonding. This peak corresponds to the peak in the CC sp^3 vibration density of states (VDOS) of ta-C in simulations[51,52] and EELS data.[65] Gilkes et al.[31] gave some empirical relations between the $I(T)/I(G)$ ratio, the T peak position and the sp^3 content, Fig. 19.

The 244-nm UV Raman spectrum is a favored means to derive the sp^3 content of amorphous carbons. This requires an understanding of how the spectrum develops with sp^3 content. For example, the variation of $I(T)/I(G)$ with the sp^3 content is quite nonlinear for 60–90 % sp^3 contents, Fig. 19(a). The spectrum possesses the large G peak. If this is subtracted, this leaves the T peak, which arises from a peak in the sp^3 VDOS. As the sp^3 content falls, the sp^3 VDOS peak at 1060 cm^{-1} shifts upwards to that of a sp^2 network at 1400 cm^{-1}.[65] A shifting T feature is also seen in the UV Raman spectra of ta-C:N with increasing nitrogen content.[34] Alternatively, the changes could be represented as a reduc-

tion of the T peak at 1060 cm^{-1} and the rise of a peak around 1400 cm^{-1}, a D-like peak. This is consistent with the discussion in Sec. III C. There we noted that a D peak can survive in UV Raman spectra of sp^2 a-C, where it becomes like a VDOS feature of sp^2 rings. Thus, as the sp^2 content of ta-C rises, the T peak intensity (corresponding to the CC sp^3 VDOS) is reduced, with a corresponding increase of a D peak. We use this model here.

A complication is that the D peak intensity depends not only on the sp^2 fraction, but also on its order. If the sp^2 sites have graphitic order, the D peak is absent in UV, if the sp^2 sites are in chains the D peak is absent, only if the sp^2 sites are in disordered rings does a residual D peak survive in UV.

This can then explain the range of $I(T)/I(G)$ values seen for high sp^3 content ta-C. This could be attributed to the sensitivity of the T peak to small changes of sp^3 content at high sp^3 content. More likely, a slightly different amount of sp^2 clustering can fill in the dip around 1400 cm^{-1} (clearly seen in the ta-C spectrum of Fig. 18), so smearing the T peak intensity. This effect should be accounted for, in principle, by introducing an extra D peak in the fitting, even in samples with low sp^2 content, but a physically meaningful fit is dif-
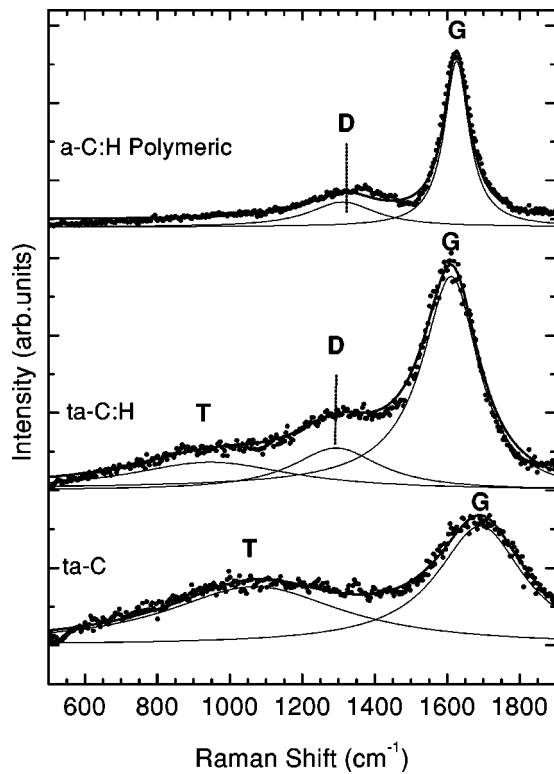
FIG. 18. UV Raman spectra of polymeric a-C:H, ta-C:H, and ta-C with the peak fits. The fitted peaks are correspondingly labeled. Note that for polymeric a-C:H a clear dip at ~1500 cm^{-1} exists between the D peak at the G peak. For ta-C:H (or diamondlike a-C:H) the residual D peak and larger G peak fill the dip around 1500 cm^{-1}.
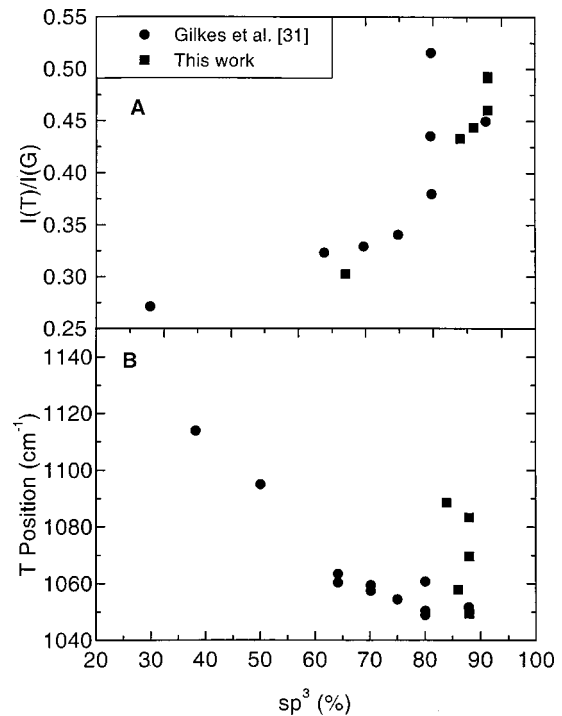

FIG. 19. (a) $I(T)/I(G)$ vs sp^3 fraction for nonhydrogenated carbon films. (b) T peak position vs sp^3 fraction for nonhydrogenated carbon films. The parameters were derived with a BWF+Lorentzian fit, thus allowing the T peak to upshift, as for Gilkes *et al.* (Ref. 31). A higher T peak position for a given sp^3 content means higher clustering of the sp^2 phase (see text).

ficult in these cases as this implies using two peaks to fit a broad feature with no clear modulations. Thus, the empirical relations of Gilkes *et al.*,[31] obtained with a simple-two-peak fit

($1T$ peak and $1G$ peak) that allows an upshift of the T peak, are useful benchmarks.

The increase of sp^2 content and clustering both tend to reduce $I(T)/I(G)$. However, the T peak disappears only for large sp^2 contents. Thus, the effect of clustering is to reduce the direct correlation between T intensity and sp^3 content. Nevertheless, we can still distinguish high sp^3 contents from low sp^3, unlike in visible Raman spectra. Indeed, a T peak around 1060 cm^{-1} and an $I(T)/I(G)$ ratio of about ~0.4–0.42 in H-free samples is a sufficient condition to estimate an sp^3 content of ~80%. An $I(T)/I(G)$ ratio of 0.3–0.4 still indicates a sp^3 content of 60–80 %, but sp^2 clustering makes it difficult to give a precise figure. Finally, $I(T)/I(G)<0.2$ indicates a sp^3 content lower than 20–30 %. Thus the presence of a T peak is a powerful qualitative means to cut through the hysteresis. Indeed, a sample with high sp^3 fraction and large hysteresis will show a T peak (even if smaller than a similar sp^3 content sample, but with limited clustering of the sp^2 phase). On the other hand, a sample with low sp^3 fraction but with the same $I(D)/I(G)$ in visible excitation will not show any T peak in the UV.

The T peak has a low-energy tail, which is really a second peak around 600 cm^{-1}.[30] This peak is present in ta-C even for visible excitation and arises from sp^2 bending modes.[66] It is seen in Fig. 1 in the 325 nm spectrum, where the signal of the Si substrate is suppressed and the T peak is only a small bump. This peak is neglected when fitting the 244-nm Raman spectra of ta-C, due to the strength of the T peak at this energy.

The analysis of T peaks extends to hydrogenated samples. Figures 2 and 6 show that the T peak in ta-C:H or a-C:H is around ~980 cm^{-1}, lower than in ta-C. This is consistent with the simulations of the C-C sp^3 VDOS in ta-C:H.[63] The presence of the residual D peak must be taken into account when fitting. As a first approximation, we use three Lorentzians to fit the spectra (Fig. 18). For hydrogenated samples, EELS gives the total amount of sp^3 bonded C atoms, in both C-C and C-H sp^3 bonds, but the T peak is sensitive only to C-C sp^3 bonds. Indeed, comparing the UV Raman spectra of ta-C:H and polymeric a-C:H (Figs. 2 and 7), it is clear that most C sp^3 atoms are bonded to H in polymeric a-C:H, due to the absence of a clear T peak, whilst in ta-C:H there is a sizable amount of C-C sp^3 bonds. Empirically, $I(T)/I(G)$ ~0.1–0.2 in (t)a-C:H indicates an overall sp^3 content of ~70%. Clearly, as sp^2 clustering also contributes to a D peak, this can make things more difficult.

Note that our approach, as for Ref. 31, is to define the intensity ratio $I(T)/I(G)$ as a peak height ratio rather than an area ratio, whilst others[34] use the area ratio. This is a prag-

matic choice. Identifying the T peak as a CC sp^3, VDOS we should take its area as the sp^3 fraction. However the T peak width is well defined only for the two-Lorentzian fit in ta-C, and it can vary significantly with fitting in a three-Lorentzian fit (as in ta-C:H, Fig. 18). Furthermore, the G peak in UV Raman represents only the sp^2 sites resonantly enhanced at that energy. Its area reflects the sp^2 quantity modulated by a different cross section for each sp^2 configuration.

A final question for the $I(T)/I(G)$ ratio in UV Raman is the cross-sectional uniformity of the sample. We noted in Sec. II A that our samples are extremely uniform in the z direction.[43] However, it is possible to have quite layered ta-C films, with surface layers thicker than the penetration depth of UV light (~ 10–15 nm).[43] In that case, UV Raman provides information on the outer part of the sample. On the other hand, this surface sensitivity can be exploited to investigate the changes induced by surface treatments.

IV. CONCLUSIONS

We have presented the dispersion of Raman peaks with varying excitation energy for a comprehensive series of amorphous carbons. We showed how most trends can be classified and explained by extending the three-stage model developed to explain the visible Raman spectra of disordered and amorphous carbons.

We showed how amorphous carbons can have a D peak even in UV excitation, in contrast to disordered graphite. We discussed the origin of the trends of the T peak with sp^3 content for hydrogenated and hydrogen-free samples. We showed how its blueshift is due to the appearance of a residual D peak, due to the vibrations of all ringlike structures, and not due to a change in the sp^3 VDOS, as sometimes suggested.

We also stress how the clustering of the sp^2 phase is the major parameter controlling the Raman spectra at any wavelength. Probing the same sample with visible and UV excitation allows us to derive the amount and clustering of sp^2 sites, at least qualitatively. This is due to the inversion of the trend of the G peak, resulting in a shift from visible to UV, which is larger for less sp^2 clustering. The appearance of the T peak gives a direct indication of the presence of sp^3 bonds. This means that a two-wavelength study (e.g., at 514 and 244 nm) can provide a fast and powerful characterization tool for amorphous and disordered carbons since the peaks' dispersion is a fingerprint that is specific to each different carbon system.

We showed how, for hydrogenated samples, CH_x stretching modes can be detected in UV Raman. Indeed UV Raman can directly detect H bonding whilst assessing the CC bonding at the same time. This could allow to derive the fraction of C sp^3 bonded to hydrogen, which is a key factor to distinguish hydrogenated samples with the same total sp^3 content.

*Email address: acf26@eng.cam.ac.uk

[1] J. Robertson, Prog. Solid State Chem. **21**, 199 (1991); Pure Appl. Chem. **66**, 1789 (1994).

[2] J. Robertson, Adv. Phys. **35**, 317 (1986).

[3] M. S. Dresselhaus, G. Dresselhaus, and P. C. Eklund, *Science of Fullerenes and Carbon Nanotubes* (Academic Press, New York, 1996).

[4] S. A. Solin and A. K. Ramdas, Phys. Rev. B **1**, 1687 (1970).

[5] F. Tuinstra and J. L. Koening, J. Chem. Phys. **53**, 1126 (1970).

[6] R. J. Nemanich and S. A. Solin, Phys. Rev. B **20**, 392 (1979).

[7] P. Lespade, A. Marchard, M. Couzi, and F. Cruege, Carbon **22**, 375 (1984).

[8] M. A. Tamor and W. C. Vassel, J. Appl. Phys. **76**, 3823 (1994).

[9] A. C. Ferrari and J. Robertson, Phys. Rev. B **61**, 14 095 (2000).

[10] A. M. Rao, E. Richter, S. Bandow, B. Chase, P. C. Eklund, K. A. Williams, S. Fang, K. R. Subbaswamy, M. Menon, A. Thess, R. E. Smalley, G. Dresselhaus, and M. S. Dresselhaus, Science **75**, 187 (1997).

[11] D. S. Bethune, G. Meijer, W. C. Tang, H. J. Rosen, W. G. Golden, H. Seki, C. A. Brown, and M. S. De Vries, Chem. Phys. Lett. **179**, 181 (1991).

[12] M. A. Pimenta, A. Marucci, S. A. Empedocles, M. G. Bawendi, E. B. Hanlon, A. M. Rao, P. C. Eklund, R. E. Smalley, G. Dressel-haus, and M. S. Dresselhaus, Phys. Rev. B **58**, R16 016 (1998).

[13] S. D. M. Brown, P. Corio, A. Marucci, M. S. Dresselhaus, M. A. Pimenta, and K. Kneipp, Phys. Rev. B **61**, R5137 (2000).

[14] A. C. Ferrari and J. Robertson, Phys. Rev. B **63**, 121405(R) (2001).

[15] J. M. Calleja, J. Khul, and M. Cardona, Phys. Rev. B **17**, 876 (1978).

[16] R. P. Vidano, D. B. Fishbach, L. J. Willis, and T. M. Loehr, Solid State Commun. **39**, 341 (1981).

[17] P. Tan, Y. Deng, and Q. Zhao, Phys. Rev. B **58**, 5435 (1998).

[18] Z. Wang, X. Huang, R. Xue, and L. Chen, J. Appl. Phys. **84**, 227 (1998).

[19] Y. Kawashima and G. Katagiri, Phys. Rev. B **52**, 10 053 (1995).

[20] K. Sinha and J. Menendez, Phys. Rev. B **41**, 10 845 (1990).

[21] A. V. Baranov, A. N. Bekhterev, Y. S. Bobovich, and V. I. Petrov, Opt. Spectrosc. **62**, 612 (1987).

[22] Y. Wang, D. C. Alsmeyer, and R. L. McCreery, Chem. Mater. **2**, 557 (1990).

[23] M. Ramsteiner and J. Wagner, Appl. Phys. Lett. **51**, 1355 (1987); J. Wagner, M. Ramsteiner, Ch. Wild, and P. Koidl, Phys. Rev. B **40**, 1817 (1989).

[24] M. Yoshikawa, G. Katagiri, H. Ishida, A. Ishitani, and T. Aka-matsu, Solid State Commun. **66**, 1177 (1988); Appl. Phys. Lett.

52, 1639 (1988); M. Yoshikawa, N. Nagai, M. Matsuki, H. Fukuda, G. Katagiri, H. Ishida, A. Ishitani, and I. Nagai, Phys. Rev. B **46**, 7169 (1992).

[25] M. A. Tamor, J. A. Haire, C. H. Wu, and K. C. Hass, Appl. Phys. Lett. **54**, 123 (1989).

[26] I. Pocsik, M. Koos, M. Hundhausen, and L. Ley, in *Amorphous Carbon: State of the Art*, edited by S. R. P. Silva *et al.* (World Scientific, Singapore, 1998), p. 224.

[27] J. Wagner, C. Wild, and P. Koidl, Appl. Phys. Lett. **59**, 779 (1991).

[28] R. W. Bormett, S. A. Asher, R. E. Witowski, W. D. Partlow, R. Lizewski, and F. Petit, J. Appl. Phys. **77**, 5916 (1995).

[29] K. W. K. Gilkes, H. S. Sands, D. N. Batchelder, J. Robertson, and W. I. Milne, Appl. Phys. Lett. **70**, 1980 (1997).

[30] V. I. Merkulov, J. S. Lannin, C. H. Munro, S. A. Asher, V. S. Veerasamy, and W. I. Milne, Phys. Rev. Lett. **78**, 4869 (1997).

[31] K. W. R. Gilkes, S. Prawer, K. W. Nugent, J. Robertson, H. S. Sands, Y. Lifshitz, and X. Shi, J. Appl. Phys. **87**, 7283 (2000).

[32] A. C. Ferrari, B. Kleinsorge, N. A. Morrison, A. Hart, V. Stolojan, and J. Robertson, J. Appl. Phys. **85**, 7191 (1999).

[33] A. C. Ferrari, B. Kleinsorge, G. Adamopoulos, J. Robertson, W. I. Milne, V. Stolojan, L. M. Brown, A. Libassi, and B. K. Tanner, J. Non-Cryst. Solids **266–269**, 765 (2000).

[34] J. R. Shi, X. Shi, Z. Sun, E. Liu, B. K. Tay, and S. P. Lau, Thin Solid Films **366**, 169 (2000).

[35] A. C. Ferrari, B. Racine, N. A. Morrison, I. Hutchings, W. I. Milne, and J. Robertson, in *Amorphous and Nanostructured Carbon*, edited by J. P. Sullivan *et al.*, MRS Symposia Proceedings No. **593** (Materials Research Society, Pittsburgh, 2000), p. 523.

[36] M. Bonelli, A. C. Ferrari, A. P. Fioravanti, A. Miotello, and P. M. Ossi, in *Amorphous and Nanostructured Carbon* (Ref. 35), p. 359.

[37] I. Pocsik, M. Hundhausen, M. Koos, and L. Ley, J. Non-Cryst. Solids **227–230**, 1083 (1998).

[38] M. J. Matthews, M. A. Pimenta, G. Dresselhaus, M. S. Dresselhaus, and M. Endo, Phys. Rev. B **59**, 6585 (1999).

[39] C. Thomsen and S. Reich, Phys. Rev. Lett. **85**, 5214 (2000).

[40] C. Mapelli, C. Castiglioni, G. Zerbi, and K. Mullen, Phys. Rev. B **60**, 12 710 (2000).

[41] C. Castiglioni, C. Mapelli, F. Negri, and G. Zerbi, J. Chem. Phys. **114**, 963 (2001); M. Rigolio, C. Castiglioni, G. Zerbi, and F. Negri, J. Mol. Struct. **563-564**, 79 (2001).

[42] M. C. Polo, J. L. Andujar, A. Hart, J. Robertson, and W. I. Milne, Diamond Relat. Mater. **9**, 663 (2000); K. B. K. Teo, J. T. H. Tsai, A. C. Ferrari, W. I. Milne, and J. Robertson,, J. Appl. Phys. **89**, 3706 (2001).

[43] A. C. Ferrari, A. Libassi, B. K. Tanner, V. Stolojan, J. Yuan, L. M. Brown, S. E. Rodil, B. Kleinsorge, and J. Robertson, Phys. Rev. B **62**, 11089 (2000).

[44] N. A. Morrison, S. E. Rodil, A. C. Ferrari, J. Robertson, and W. I. Milne, Thin Solid Films **337**, 71 (1999).

[45] N. M. J. Conway, A. C. Ferrari, A. J. Flewitt, J. Robertson, W. I. Milne, A. Tagliaferro, and W. Beyer, Diamond Relat. Mater. **9**, 765 (2000).

[46] A. Ilie, A. C. Ferrari, T. Yagi, and J. Robertson, Appl. Phys. Lett. **76**, 2627 (2000).

[47] X. L. Peng and T. W. Clyne, Thin Solid Films **312**, 207 (1998).

[48] I. Pocsik, M. Koos, S. H. Moustafa, J. A. Andor, O. Berkesi, and M. Hundhausen, Mikrochim. Acta **14**, 755 (1997).

[49] B. Popescu, C. Verney, E. A. Davis, V. Paret, and A. Brunet-Bruneau, J. Non-Cryst. Solids **266–269**, 778 (2000).

[50] A. C. Ferrari (unpublished).

[51] T. Kohler, T. Frauenheim, and G. Jungnickel, Phys. Rev. B **52**, 11 837 (1995).

[52] D. A. Drabold, P. A. Fedders, and P. Strumm, Phys. Rev. B **49**, 16 415 (1994).

[53] N. A. Marks, D. R. McKenzie, B. A. Pailthorpe, M. Bernasconi, and M. Parrinello, Phys. Rev. B **54**, 9703 (1996).

[54] M. Gussoni, C. Castiglioni, and G. Zerbi, in *Spectroscopy of Advanced Materials*, edited by R. J. Clark and R. E. Hester (Wiley, New York, 1991), p. 251.

[55] E. Ehrenfreund, Z. Vardeny, O. Brafman, and B. Horovitz, Phys. Rev. B **36**, 1535 (1987).

[56] V. Hernandez, C. Castiglioni, M. Del Zoppo, and G. Zerbi, Phys. Rev. B **50**, 9815 (1994).

[57] J. Ristein, R. T. Stief, L. Ley, and W. Beyer, J. Appl. Phys. **84**, 3836 (1998).

[58] R. Rumelfanger, S. A. Asher, and M. B. Perry, Appl. Spectrosc. **42**, 267 (1988); Z. Chi, X. G. Chen, J. S. W. Holtz, and S. A. Asher, Biochemistry **37**, 2854 (1998).

[59] G. Herzberg, *Molecular Spectra and Molecular Structure II* (Van Nostrand, Princeton, NJ, 1945); F. R. Dollish, W. G. Fateley, and F. F. Bentley, *Characteristic Raman Frequencies of Organic Compounds* (Wiley, New York, 1974).

[60] B. Dishler, in *Amorphous Hydrogenated Carbon Films*, edited by P. Koidl and P. Oelhafen EMRS Symposia Proceedings Vol. 17 (Les Editiones de Physisque, Paris, 1987), p. 189.

[61] A. C. Ferrari and S. E. Rodil (unpublished).

[62] P. J. R. Honeybone, R. J. Newport, J. K. Walters, W. S. Howells, and J. Tomkinson, Phys. Rev. B **50**, 839 (1994).

[63] F. Mauri and A. Del Corso, Appl. Phys. Lett. **75**, 644 (1999).

[64] M. M. M. Bilek, D. R. McKenzie, D. G. McCulloch, and C. M. Goringe, Phys. Rev. B **62**, 3071 (2000).

[65] G. P. Lopinski, V. I. Merkulov, and J. S. Lannin, Appl. Phys. Lett. **69**, 3348 (1996).

[66] W. S. Bacsa, J. S. Lannin, D. L. Pappas, and J. J. Cuomo, Phys. Rev. B **47**, 10 931 (1993).

[67] P. A. Temple and C. E. Hathaway, Phys. Rev. B **7**, 3685 (1973).

[68] F. Li and J. S. Lannin, Appl. Phys. Lett. **61**, 2116 (1992).